



This is a repository copy of *Insights into the regulation of the mitochondrial inheritance and trafficking adaptor protein Mmr1 in saccharomyces cerevisiae*.

White Rose Research Online URL for this paper:

<https://eprints.whiterose.ac.uk/214790/>

Version: Published Version

Article:

Nayef, N., Ekal, L. orcid.org/0000-0001-8916-4201, Hetteema, E.H. orcid.org/0000-0003-2245-5287 et al. (1 more author) (2024) Insights into the regulation of the mitochondrial inheritance and trafficking adaptor protein Mmr1 in saccharomyces cerevisiae. *Kinases and Phosphatases*, 2 (2). pp. 190-208. ISSN 2813-3757

<https://doi.org/10.3390/kinasesphosphatases2020012>

Reuse

This article is distributed under the terms of the Creative Commons Attribution (CC BY) licence. This licence allows you to distribute, remix, tweak, and build upon the work, even commercially, as long as you credit the authors for the original work. More information and the full terms of the licence here:

<https://creativecommons.org/licenses/>

Takedown

If you consider content in White Rose Research Online to be in breach of UK law, please notify us by emailing eprints@whiterose.ac.uk including the URL of the record and the reason for the withdrawal request.



eprints@whiterose.ac.uk
<https://eprints.whiterose.ac.uk/>

Article

Insights into the Regulation of the Mitochondrial Inheritance and Trafficking Adaptor Protein Mmr1 in *Saccharomyces cerevisiae*

Nourah Nayef¹, Lakhan Ekal^{1,2} , Ewald H. Hettema¹  and Kathryn R. Ayscough^{1,*} 

¹ School of Biosciences, University of Sheffield, Western Bank, Sheffield S10 2TN, UK; nyynayef1@sheffield.ac.uk (N.N.); lakhan.ekal@embl-hamburg.de (L.E.); e.hettema@sheffield.ac.uk (E.H.H.)

² European Molecular Biology Laboratory, 22607 Hamburg, Germany

* Correspondence: k.ayscough@sheffield.ac.uk

Abstract: Mitochondria are organelles involved in cellular energetics in all eukaryotes, and changes in their dynamics, fission, fusion, or localization can lead to cell defects and disease in humans. Budding yeast, *Saccharomyces cerevisiae*, has been shown to be an effective model organism in elucidating mechanisms underpinning these mitochondrial processes. In the work presented here, a genetic screen was performed to identify overexpressing kinases, phosphatases, and ubiquitin ligases, which resulted in mitochondrial defects. A total of 33 overexpressed genes showed mitochondrial phenotypes but without severe growth defects. These included a subset that affected the timing of mitochondrial inheritance and were the focus of further study. Using cell and biochemical approaches, the roles of the PAK-family kinase Cla4 and the E3-ubiquitin ligases Dma1 and Dma2 were investigated. Previous studies have indicated the roles of kinase Cla4 and ligases Dma1 and Dma2 in triggering the degradation of trafficking adaptors in the bud, which leads to disruption of the interaction with the transporting class V myosin, Myo2. Here, we map a key interface between Cla4 and the mitochondrial adaptor Mmr1 necessary for phosphorylation and identify a region of Mmr1 required for its degradation via Dma1 and Dma2. Together, our data provide insights into key regulatory regions of Mmr1 responsible for its function in mitochondrial inheritance.

Keywords: organelle inheritance; mitochondria; kinase; ubiquitin ligase; Mmr1; *Saccharomyces cerevisiae*; PAK



Citation: Nayef, N.; Ekal, L.; Hettema, E.H.; Ayscough, K.R. Insights into the Regulation of the Mitochondrial Inheritance and Trafficking Adaptor Protein Mmr1 in *Saccharomyces cerevisiae*. *Kinases Phosphatases* **2024**, *2*, 190–208. <https://doi.org/10.3390/kinasesphosphatases2020012>

Academic Editor: Mauro Salvi

Received: 8 May 2024

Revised: 5 June 2024

Accepted: 13 June 2024

Published: 18 June 2024



Copyright: © 2024 by the authors. Licensee MDPI, Basel, Switzerland. This article is an open access article distributed under the terms and conditions of the Creative Commons Attribution (CC BY) license (<https://creativecommons.org/licenses/by/4.0/>).

1. Introduction

Eukaryotic cells are subdivided into membrane-bound organelles, with each organelle having a distinct structure and function. During a successful cell division, organelles are usually distributed by a mechanism coordinated with nuclear division and eventual cytokinesis. The process of organelle sharing with daughter cells is often referred to as organelle inheritance. The budding yeast, *Saccharomyces cerevisiae*, has been used extensively to increase understanding of fundamental cell biological processes. In the case of organelle inheritance, the molecular mechanism of yeast organelle transport has been well characterized and similar conserved processes have been found for organelle transport in humans [1–5]. In yeast, some organelles such as peroxisomes and vacuoles are usually transported to the growing daughter cell but they can also be synthesized de novo [1,6,7]. Such organelle biogenesis is observed in situations of impaired or mutagenized trafficking. Mitochondria, however, cannot be generated de novo and inheritance by the growing daughter cell is essential [8–10].

The mechanism of organelle inheritance in budding yeast has general features, with each organelle harbouring a specific protein called an adaptor on its surface that is recognized by a type V myosin motor protein. The interaction between the adaptor and the myosin facilitates the movement of that organelle towards the bud along actin filaments [11,12]. *S. cerevisiae* expresses two class V myosin motors, Myo2 and Myo4 [13].

Myo4 has been shown to be involved in transporting cortical endoplasmic reticulum (cER) [14] and specific mRNA molecules [15]. Myo2 is involved in the movement of most membrane-bound organelles: secretory vesicles [16,17], the vacuole/lysosome [18–20], late Golgi [21], mitochondria [22], and peroxisomes [23].

In yeast, these organelles have been proposed to follow similar stages of movement: (1) association of organelle and myosin in the mother cell; (2) transport of the organelle by the myosin along tracks of actin filaments from the mother to the bud; and (3) release of the organelle in the bud preventing its movement back to the mother cell [1,3,5]. Studies on organelle inheritance indicate a common pathway of regulation for ensuring organelles remain in the bud following transport. In the case of vacuoles and peroxisomes where more research has been carried out, the adaptor proteins Vac17 and Inp2, respectively, bind to Myo2 in the mother cell, but at the bud tip they are phosphorylated by the PAK (p21-activated kinase)-family kinase Cla4. This phosphorylation event then makes the adaptor proteins a target for ubiquitination by the E3 ligases Dma1 and Dma2, which leads to their subsequent degradation [12,24–27]. More recently, it has been demonstrated that mitochondrial Mmr1 can also be phosphorylated by Cla4 and then ubiquitinated by Dma1 and Dma2, leading to its degradation [27,28].

Mitochondria are the organelles in the cell where adenosine triphosphate (ATP) is generated through the process of oxidative phosphorylation as well as being the sites of production of intermediary metabolites, such as acetyl-CoA and NAD⁺/NADH. Both transport and retention of mitochondria are particularly important as the mother and daughter cells must contain sufficient high-quality organelles at cytokinesis to ensure faithful inheritance to future generations of cells [29]. Recent studies also show that damaged mitochondria are selectively retained in mother cells, which ensures that at cytokinesis the daughter cells have only received fully functional mitochondria [30]. Possibly reflecting the importance of inheritance, there appear to be at least two partially redundant routes to transport mitochondria: one involving the adaptor Mmr1 and the other using Ypt11, which is also involved in the transport of the late Golgi compartments and potentially E.R. [31–35]. Both pathways, however, use the same Myo2 myosin motor. A temperature-sensitive strain of Myo2 (*myo2-34*) is compromised in binding Ypt11 [31,36], whereas the *myo2-573* temperature-sensitive mutant was shown to not interact with Mmr1 [32]. In both cases, mutations delay but do not completely inhibit mitochondrial inheritance. In addition, the deletion of *gem1* (encoding the homologue of the mammalian mitochondrial Miro-GTPase), shows synthetic enhancement of an *MMR1* deletion, suggesting some redundancy, though Gem1 itself has not been shown to bind directly to Myo2 [35].

As well as these adaptor proteins binding to myosin, there is machinery that is required to tether mitochondria to ensure that high-quality mitochondria remain in the mother cell as well as being transported to the bud. Mfb1 is a protein that localizes to the tip of the mother cell opposite the growing bud. Deletion of *MFB1* causes loss of the mother tip mitochondrial population and leads to defects in mitochondrial function and premature replicative ageing [29,37]. Another key protein in controlling mitochondrial distribution is Num1, which has been shown to interact with the integral mitochondrial protein, Mdm36, to form a complex called MECA (mitochondria ER–cortex anchor), which is required for the anchoring of mitochondria to the plasma membrane [37,38]. The machinery involved in tethering and transport also interacts with other complexes involved in fusion and fission. Together, these processes are critical for managing mitochondrial homeostasis such that new mitochondria are generated and defective organelle material is degraded through mitophagy.

While much research has focused on the role of microtubules in the transport of mitochondria in mammalian cells, there is a growing body of research highlighting the importance of actin-based interactions including roles for myosin motors in governing mitochondrial dynamics [39]. In particular, the mammalian myosins, MYO5 and MYO19, have been shown to transport mitochondria [40,41], while a MYO6 interaction is important during mitophagy [42]. Defects in mitochondrially associated myosins have been linked to a

number of human disorders, including Griscelli syndrome (linked to MYO5 mutations) and hearing impairments (mutations in MYO6 and MYO19) [39]. How mitochondria become both associated with, and released from, myosins at appropriate times and locations in cells is essential for cell health but is not well understood. Gaining a deeper understanding of the process in a model organism has the potential to generate new insights that can focus future research on more complex cell types.

2. Results

2.1. A Genetic Screen to Identify Possible Regulators of Mitochondrial Inheritance

An over-expression kinase, phosphatase, and ubiquitin ligase library were screened to identify genes that, when overexpressed, affect mitochondrial inheritance [43]. The library strains were crossed individually with a strain carrying a mitochondrial marker (Mdh1-mNG) to generate diploid strains, which were screened manually for altered mitochondrial morphology or distribution. Of the 500 genes tested in the library screen, 90 showed some mitochondrial phenotypes, but the majority of these also showed other gross morphological defects. Gene Ontology information in the *Saccharomyces* Genome Database (<https://www.yeastgenome.org/>, accessed on 25 January 2023) was used to determine which of the 90 gene-encoded proteins had any evidence linking to mitochondrial function or had mitochondrial defects in the absence of severe sickness or other growth defects. This led to 33 strains carrying overexpressing genes being selected for further analysis (listed in Table 1; shown in Figure S1). These were first re-crossed to verify phenotypes before being analysed further. It was noted that two of the genes (*CQD1* and *MCP2*) encode proteins that localize to the mitochondrial inner membrane. It is possible that the N-terminal mCherry tag could interfere with signal motifs required for uptake to the mitochondria. Amongst the screen isolates, it was noted that overexpression of both *CLA4* and *DMA1* showed a delay in mitochondrial inheritance to the bud. These genes have been shown to work in the pathway leading to the degradation of organelle adaptors in buds, which ensures unidirectional organelle transport during bud growth [3,5]. It was also observed that overexpression of the spindle position checkpoint (SPoC) kinase, *KIN4*, led to an accumulation of mitochondria at the bud tip.

In thirteen strains, defects in mitochondrial inheritance were observed as either a delay in mitochondrial inheritance in early buds (*CLA4*, *BUL2*, *DMA1*, *CDC26*, *UBC9*, *VID30*, *ARP5*, *MSG5*, *NCS2*, *OCA6*, *PPN2*) or as an increase in mitochondria at the tip of large buds (*PCL7*, *KIN4*), though it was noted that, in most cases, the delayed inheritance phenotype was not highly penetrant with $\leq 25\%$ of cells showing the phenotype. In strains with the most robust inheritance phenotypes, we then investigated whether the gene overexpression could be linked to a change in localization or level of the mitochondrial trafficking adaptor, Mmr1. Strains overexpressing relevant genes were crossed with a strain expressing fluorescently tagged Mmr1-mNG and analysed microscopically. An overexpressed kinase (*CLA4*), ubiquitin ligases (*BUL2*, *DMA1*), and overexpressed phosphatase *MSG5* resulted in a visible reduction in the level of Mmr1 in the bud. In contrast, overexpression of *KIN4* and *PCL7* led to an accumulation of Mmr1 at the tips of large buds compared to that in wild-type cells. Figure 1 shows representative examples of gene overexpression leading to changes in Mmr1 distribution compared to wild-type cells.

Table 1. Genes that affect the mitochondrial phenotype when overexpressed. Mitochondrial morphology and localization were analysed by visualizing the mNeonGreen (mNG)-tagged mitochondrial reporter Mdh1 protein. The phenotypes were scored as to whether they appeared normal (like wild-type phenotypes with long, polarized strands often crossing the mother–bud neck in medium-budded cells) or abnormal. ‘Fragmented’ was used as a descriptor to encompass phenotypes with fewer long strands of mitochondria and more spots, though these can be varied in number and distribution. Gene descriptions are from www.yeastgenome.org (accessed on 2 March 2024).

Overexpressed Gene Kinases or Associated Subunits	Mitochondrial Phenotype	Gene Description
<i>CLA4</i>	Inheritance delay, fragmented, absence at mother–bud neck	Involved in septin ring assembly and organelle inheritance.
<i>CLB4</i>	Abnormal accumulations, often at the tips	Regulates mitotic spindle assembly and spindle pole body separation.
<i>GAL83</i>	Fragmented	Galactose metabolism is part of the Snf kinase complex.
<i>KIN4</i>	Fragmented, accumulation at the tip	Inhibits the mitotic exit network when the spindle position checkpoint is activated.
<i>CQD1</i>	Fragmented with accumulations at the periphery of cells	UbiB protein kinase-like; role in mitochondrial organization; and localizes to inner mitochondrial membrane
<i>MCP2</i>	Abnormal	Homology to ADCK1; mitochondrial inner membrane protein required for normal morphology.
<i>PCL2</i>	Fragmented, increased mitochondria, absence at mother–bud neck	Cyclin partner of Pho85; involved in septin ring organization and maintenance of cell polarity.
<i>PCL7</i>	Fragmented, accumulation at large bud tip and neck	Cyclin associates with Pho85, which phosphorylates Mmr1.
<i>RCK1</i>	Weaker signal, more fragmented	Kinase involved in stress response
<i>SPS1</i>	Fragmented, absence at mother–bud neck	for the positive regulation of prospore membrane formation; Ste20-family kinase.
<i>TDA1</i>	Fragmented	Unknown function.
<i>YCK2</i>	stronger signal, absence at mother–bud neck	Protein serine/threonine casein kinase1 family involved in cell morphogenesis.
<i>YPK2</i>	Stronger signal, abnormal organization	AGC type kinase; phosphorylation of Myo5 motor domain; and enables motor activity.
Ubiquitin ligases or those associated with ubiquitination		
<i>BUL2</i>	Inheritance delay (<25%), fragmented, absence at mother–bud neck	α -arrestin part of Rsp5 E3 ubiquitin ligase complex.
<i>CDC26</i>	Inheritance delay, fragmented	Part of APC ubiquitin protein ligase, and is required for the degradation of anaphase inhibitors, including mitotic cyclins.
<i>DMA1</i>	Inheritance delay (<25%), fragmented, absence at mother–bud neck	E3 family, involved in spindle position checkpoint with paralog Dma2.
<i>PTH2</i>	Fragmented	Mitochondrial aminoacyl-tRNA hydrolase;
<i>RPL40B</i>	Inheritance delay (<25%)	facilitates the assembly of ribosomal protein into ribosomes.
<i>SKP1</i>	Fragmented, absence at mother–bud neck	Component of SCF ubiquitin ligase complex.
<i>SKP2</i>	Fragmented, absence at mother–bud neck	F-box protein of unknown function predicted to be part of SCF complex.
<i>TOM1</i>	Fragmented, possible mother tethering defect	E3 ubiquitin ligase is required to target Cdc6 for ubiquitin-mediated destruction during G1 phase.
<i>UBC9</i>	Inheritance delay (<25%), fragmented	SUMO-conjugating enzyme required for cyclin degradation.
<i>UBX7</i>	Fragmented, absence at mother–bud neck	UBX (ubiquitin regulatory X) domain-containing protein.
<i>UFO1</i>	Mitochondria extending around the distal mother pole	Subunit of Skp1-Cdc53-F-box receptor (SCF) E3 ubiquitin ligase complex.
<i>VID30</i>	Inheritance delay (<25%), fragmented	GID subunit ubiquitin ligase complex is involved in proteasome-mediated protein catabolism.
Other genes		
<i>ARP5</i>	Inheritance delay (<25%), fragmented	Involved in chromatin remodelling and nucleosome mobilization.
<i>MSG5</i>	Inheritance delay (<25%), fragmented	Dual-specificity protein phosphatase is involved in cell wall organization or biogenesis.
<i>NCS2</i>	Inheritance delay (<25%), fragmented	Involved in tRNA wobble uridine thiolation.
<i>NTA1</i>	Fragmented, possible mother tethering defect	Amidohydrolase is involved in protein catabolism; localizes to mitochondria.
<i>OCA6</i>	Inheritance delay (<25%), absence at mother–bud neck	Unknown function.
<i>PPN2</i>	Inheritance delay (<25%), fragmented	Involved in polyphosphate catabolism.
<i>SGT1</i>	Fragmented	Involved in assembly and nuclear export of the ribosomal large subunit and translation.
<i>YIL001w</i>	Fragmented, absence at the mother–bud neck, possible mother tethering defect	Unknown function.

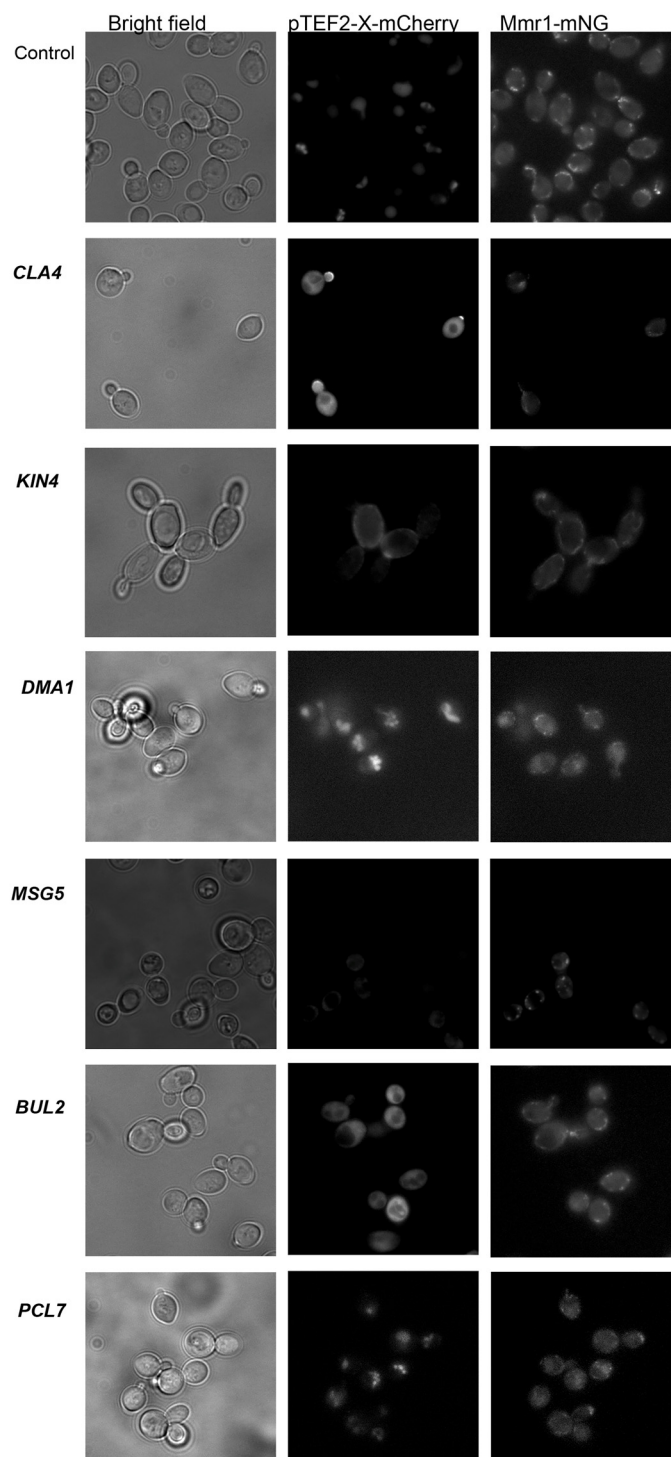


Figure 1. Genes that affect Mmr1 when overexpressed. Shown are bright field (left) and fluorescence cell images (central and right) from crosses of strains overexpressing genes as an mCherry fusion under TEF2 promoter and Mmr1-mNG.

2.2. Overexpression of *CLA4* Reduces *Mmr1* Levels

The screen and subsequent Mmr1 localization analysis revealed that elevated *CLA4* can disrupt mitochondrial inheritance, though the delay in inheritance was only clearly observed in small-budded cells. A reduction in Cla4 levels in a *ste20* null background has previously been shown to lead to an increase in Mmr1 levels [27]. To determine whether *CLA4* overexpression effect on delayed inheritance of mitochondria is potentially

due to its effects on Mmr1, we analysed the levels of Mmr1 in wild-type cells and those overexpressing *CLA4*. To ensure that effects were not related to overexpression from the *TEF2* promoter, *CLA4* was cloned into a plasmid with an alternative high-level expression promoter *TPI* (pNN6). As shown in Figure 2, overexpression of *CLA4* correlates with a reduction in Mmr1 levels, which could be part of a mechanism leading to the observed delay in mitochondrial transport to growing buds of cells.

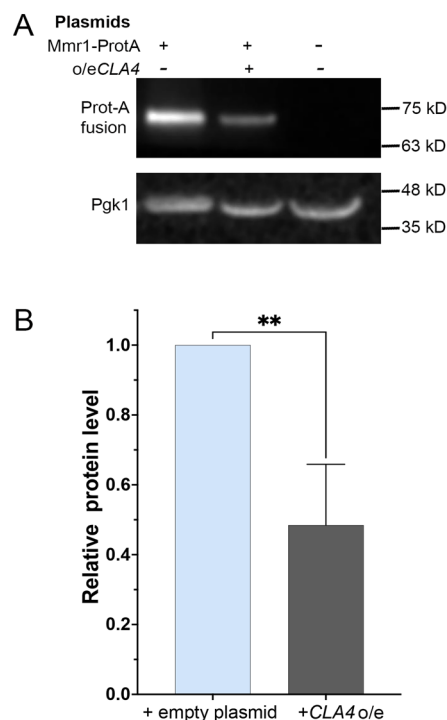


Figure 2. Effect of *CLA4* overexpression on Mmr1. Yeast strains with plasmids expressing Mmr1–Protein A and also carrying an empty plasmid or a *pTPI-CLA4* overexpression plasmid were grown to log phase. Protein extracts were produced and separated by SDS-PAGE and then blotted onto PVDF. (A) Membranes were probed with antibodies to Protein A or to Pgk1 as a loading control. (B) Three blots were analysed using densitometry to compare the effect of *CLA4* overexpression on Mmr1. The levels relative to wild-type levels were plotted. The graph shows average values with standard deviation. The significance of $p < 0.0069$ (denoted **) was determined using the two-tailed unpaired Student's *t*-test.

The Cla4 kinase has generally been considered to be active within the bud rather than the mother cell [26,44]. To further our understanding of the location and role of the Cla4 phosphorylation of Mmr1 in mitochondrial transport, we sought to generate Mmr1 mutants inhibited in their interaction with Myo2. We hypothesized that disruption of the Myo2–Mmr1 interaction could lead to Mmr1 remaining in the mother cell, as has been shown by Myo2-binding mutants of the peroxisomal receptor Inp2 [45]. This would allow us to determine whether *CLA4* overexpression was impacting the mother cell domain, where it has previously been postulated that organelle adaptors would be protected [24,28,46]. A previous study demonstrated that a Myo2 I1308A mutation caused a strong inhibition of Mmr1 binding and also reduced mitochondrial transport to the bud [32]. To avoid possible disruption of other cargoes binding through Myo2 mutation, we took advantage of the mutational analysis previously carried out by Tang and colleagues [28]. In their study, the residues R409 and L410 were separately and together mutagenized. A single mutation R409E was sufficient to inhibit the binding of an Mmr1 peptide (398–430) to the Myo2-cargo-binding domain when analysed using Isothermal calorimetry.

First, we investigated Mmr1–Myo2 binding using biochemical assays. As described in Section 4, the Myo2-cargo-binding tail fused to GST was expressed and bound to

glutathione beads. The Mmr1 fragment (residues 378–430) was expressed as an MBP fusion and eluted from beads. This region contains the previously identified binding site [28,32]. GST alone on beads was used as a negative control. As shown in Figure 3, the Arg-Glu charge swap mutation at residue 409 does indeed reduce the binding of Mmr1 to the Myo2-cargo-binding domain. While some residual binding was observed, the fragment also showed a low level of binding to GST alone on beads. Because we were interested in the *in vivo* consequences of the mutation, we then used a yeast two-hybrid assay to determine whether the Mmr1 R409E mutation also impacts the interaction between full-length Myo2 and Mmr1 proteins in cells. Beta-galactosidase assays were performed on strains carrying yeast two-hybrid constructs as described in Section 4. As shown in Figure 3B, the Mmr1 R409E mutation does reduce the level of interaction with Myo2, though this is about a 50% reduction rather than complete inhibition.

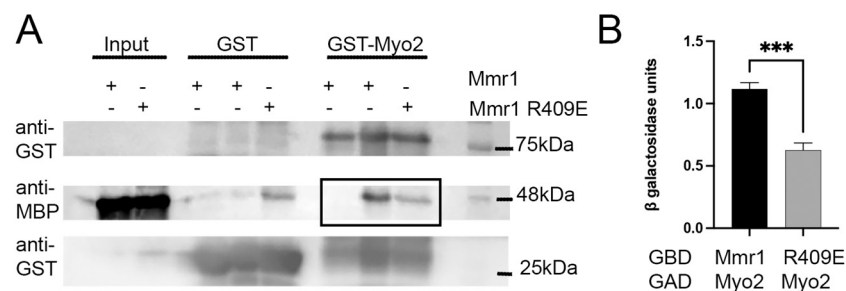


Figure 3. The R409E mutation in Mmr1 reduces binding to Myo2. (A) Mmr1 and Mmr1 R409E fragments (residues 378–430) were expressed as MBP fusions and incubated with either GST beads alone or with a Myo2-cargo-binding domain–GST fusion. After transferring to membranes, the blots were cut into three sections. Upper and lower panels were probed with anti-GST antibodies and the central part with anti-MBP. The boxed area indicates the lanes showing the binding of MBP1 fusions to GST-Myo2. (B) Strains carrying bait (full-length Mmr1 and Mmr1-R409E) and prey (Myo2) yeast two-hybrid constructs were tested for beta-galactosidase activity as a test for protein interactions as described. Three independent assays from different protein preparations were performed. The significance of $p = 0.0004$ (denoted ***) was determined using the unpaired Student's *t*-test.

To determine the impact of the mutation on Mmr1 in cells, yeast strains were then generated, which carried Mmr1-GFP and Mmr1 R409E-GFP. Images in Figure 4A show the localization of Mmr1 in cells expressing wild-type Mmr1-GFP and Mmr1 R409E-GFP. Unexpectedly, Mmr1 R409E-GFP was in buds and appeared to primarily localize at the tip of the buds. The localization of mitochondria to the tips of buds (co-incident with Mmr1-GFP) for cells expressing both wild-type and Mmr1 R409E was verified using the mitotracker strain (Figure S2). Quantification of the localization of the mutant to tips of medium- and large-budded cells is shown in Figure 4B. In addition, there appeared to be an accumulation of the mutant at the tip. The fluorescence intensity of Mmr1-GFP and Mmr1-R409E fluorescence was also measured and is shown in Figure 4C.

The increase in fluorescence intensity suggested the possibility that the Mmr1 R409E is more stable, even though it is in the bud where it would be expected to be degraded through the actions of Cla4, the ubiquitin ligases Dma1 and Dma2, and the proteasome machinery. To determine whether Mmr1 R409E is indeed more stable, protein levels following cycloheximide (0.1 mg/mL) addition to cultures were analysed at specified time points. Cycloheximide blocks new protein synthesis through action on translocation during protein translation. This allows analysis of only pre-existing proteins to be analysed. As shown in Figure 4D,E, Mmr1 R409E is significantly more stable than the wild-type protein. A decay curve was plotted from experimental repeats, which indicated a half-life of 24.9 min for Mmr1. A half-life could not be calculated for Mmr1 R409E as there was insufficient degradation in the time course.

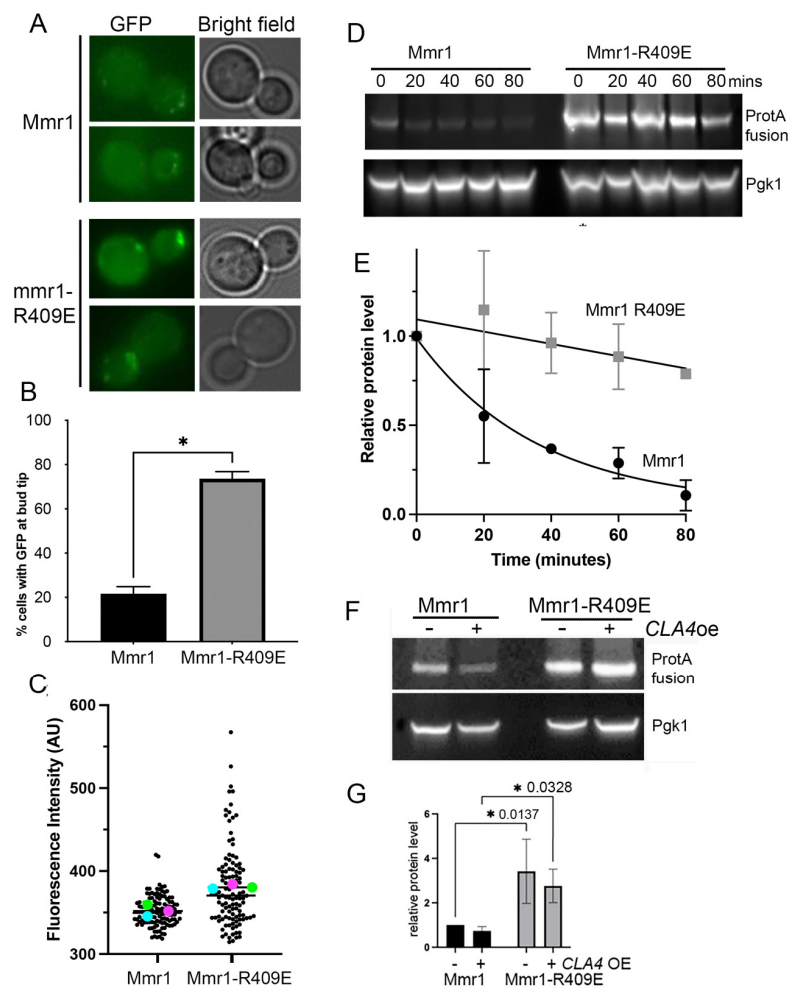


Figure 4. The effect of the Mmr1 R409E mutation. (A) Fluorescence microscopy of cells expressing wild-type Mmr1-GFP or Mmr1 R409E-GFP. (B) Analysis of % of cells in three independent cultures with clear GFP signals at the tip of medium- or large-budded cells. (C) Analysis of intensity of fluorescence at cell tips. Unpaired *t*-test $p = 0.0027$. (D) Cycloheximide was added to log phase cells expressing Mmr1-Protein A or Mmr1 R409E-Protein A and samples were taken for cell extracts at 20 min intervals. Extracts were separated on gels, blotted, and probed with antibodies to Protein A. Pgk1 levels were used as a loading control. (E) Normalising protein levels for each protein at $t = 0$ data were analysed. The graph shows simple exponential decay curves. R^2 for Mmr1 0.9023. (F) The effect of overexpressing *CLA4* on Mmr1 and Mmr1 R409E was assessed using extracts from relevant strains and Western blot analysis using antibodies to detect Protein A fusions and Pgk1. (G) Quantification of protein levels from cells in (F) relative to Mmr1 levels in wild-type cells. * indicates a p value of $n = 2$.

Given that we had already observed that overexpression of *CLA4* leads to reduced Mmr1 levels, we also investigated the effect of overexpressing *CLA4* in strains expressing Mmr1 R409E carrying a Protein A tag. As shown in Figure 4F,G, the mutation is also stable in the presence of high levels of *CLA4* that lead to increased degradation of wild-type Mmr1.

2.3. Insight into the Structural Impact of the Mmr1 R409E Mutation

Cla4 has been shown to phosphorylate Mmr1 at residue Serine 414, which is very close to the Myo2-interacting residue R409 [27]. We next considered whether the reason for the increased stability of the Mmr1 R409E mutant could be due to it impacting phosphorylation via *Cla4*. Attempts were made to purify active *Cla4* for an in vitro kinase assay but we were not able to produce sufficient active protein. Instead, we used an in silico approach

using coordinates from the Mmr1-Myo2 structure solved experimentally by X-ray crystallography (pdb 6IXP—structure of the Myo2-cargo-binding domain (residues 1153–1574) in association with Mmr1 (residues 378–441)) [28]. We used PyMol to determine the potential impact of the Mmr1 R409E mutation on protein surfaces in the relevant region of the Mmr1-Myo2 complex. As shown in Figure 5A, the introduction of a glutamate residue in place of arginine at position 409 in Mmr1 causes a dramatic change in the electrostatic landscape close to the position of the Serine 414 residue. Compared to the wild-type model, an R409E introduces a marked area of positive charge (red) close to Serine 414, which would be likely to impact the interaction surface presented to Cla4.

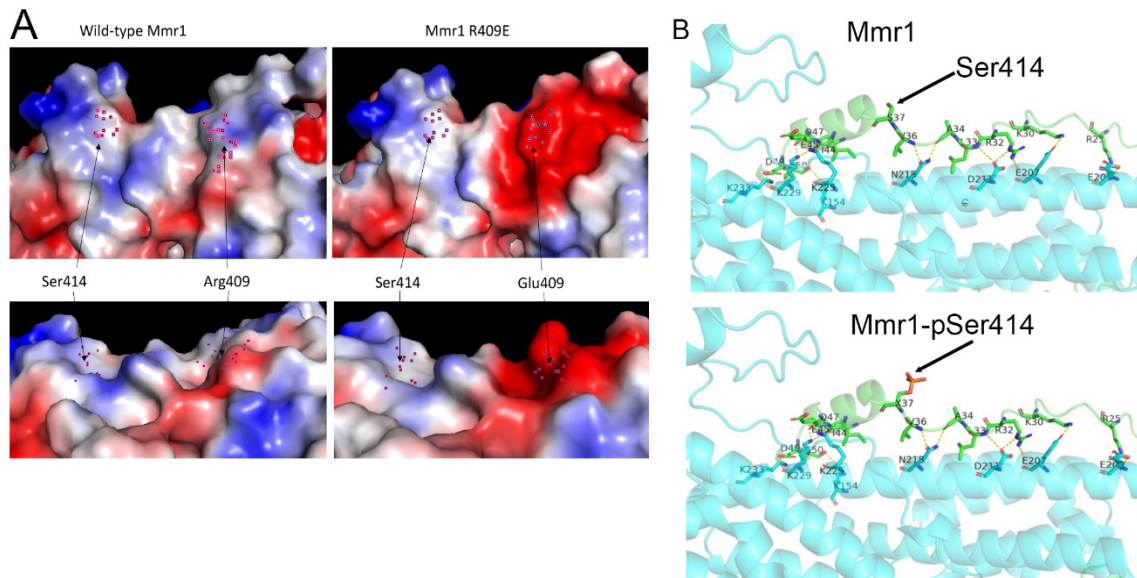


Figure 5. Changes to the electrostatic landscape of Mmr1 caused by the R409E mutation. (A) PyMol was used to analyse the effect of the R409E mutation in the context of the electrostatic surface of Mmr1. The original pdb file used 6IXP from the X-ray diffraction structure of the Myo2-cargo-binding domain (residues 1153–1574) with Mmr1; residues 378–430 are shown in the model. Blue shading denotes areas of positive charge and red areas of negative charge. Images on the left are the wild-type protein in a top-down and side-on view and the Mmr1 R409E mutant is on the right. The position of the 409 residues (R or E) and the Serine 414 residue are shown. (B) Show ribbon cartoon at the binding face of Myo2 (light blue ribbon) and Mmr1 (green). The arrow indicates the position of Serine 414. Interacting residues are numbered according to position in peptides used in the analysis (Mmr1 peptide sequence S414/S37 is in red, VLKKLTESSAVVATSTSKTEGNSARIPCKPTRLARVSVLDLKKIEEQPDSSG).

In the *in silico* studies, we also addressed whether the reported phosphorylation of Mmr1 by Cla4 would be likely to disrupt the interaction with Myo2, leading to subsequent recognition of the adaptor protein alone by ubiquitination machinery, or whether the phosphorylated Mmr1 would be predicted to remain bound to Myo2, with subsequent recognition by Dma1 of Mmr1 still in complex with Myo2. As shown in Figure 5B, the addition of a phosphate group to Ser414 (Ser 37 in modelled peptide) is expected to be oriented away from the rest of the complex and so would suggest that phosphorylation of Mmr1 Ser414 is unlikely to disrupt binding to Myo2. This also fits with other observations in which deletion of *DMA1* and *DMA2* leads to accumulation of organelles at the mother-bud neck in large-budded cells, as would be expected if they were still associated with Myo2 on actin filaments re-oriented towards the cytokinetic ring ([27]; Figure S3).

2.4. Mapping Functional Regions of the Mmr1 Dma1 Interaction

In the screen, we also identified that overexpression of the E3 ubiquitin ligase *DMA1* led to a delay in mitochondrial inheritance in small-budded cells. Given the known links

between Cla4 and Dma1 in spatial control of organelle transport, we also analysed this interaction further. The previously reported work of Obara and colleagues [27] demonstrated that deletion of *dma1* and its paralog *dma2* leads to increased levels of Mmr1, supporting the idea that Dma1 and Dma2 together are involved in ubiquitination and degradation via the proteasome. We generated a *dma1Δdma2Δ* strain and confirmed higher levels of Mmr1 and also that Mmr1 becomes localized at the neck region (Figure S3). We then sought to identify the regions of Mmr1 that were necessary for degradation. The cognate vacuole adaptor Vac17 has PEST sequences that target proteins for degradation [26]. Furthermore, Dma1 and Dma2 have forkhead-associated (FHA) domains, and in other proteins, these have been shown to bind TXXI/L or TXXD motifs [44]. We analysed the Mmr1 protein for a prediction of PEST regions and for possible Dma1- and Dma2-binding sites (Figure S4A). The C-terminal region (residues 430–491) of Mmr1 has three putative Dma1/2-binding sites and a high prediction for a PEST sequence (Figure 6A). A truncated Mmr1 mutant was generated lacking the C-terminal 61 amino acids. The truncation did not cause any major changes to mitochondrial morphology and mitochondria could be observed to localize to small buds (Figure S4B). We then determined whether the truncated Mmr1 was resistant to elevated levels of Dma1; strains were generated that expressed only full-length or truncated Mmr1, which were both tagged with Protein A. The strains were then transformed with plasmids that overexpress *DMA1*. Cell extracts were produced as described, separated, and blotted onto membranes, which were probed with anti-Protein A for Mmr1 (upper panel) or with anti-Pgk 1 (lower panel) as a loading control (Figure 6B). The band densities were measured and the ratio of Protein A and Pgk1 within single samples was used to assess the relative levels of Mmr1 and Mmr1(1–430). As shown in Figure 6C, the truncated Mmr1(1–430) shows a 3.9-fold increase in level compared to the full-length Mmr1, indicating the importance of the C-terminus in the turnover of the protein. This is similar to the 3.2 ± 0.9 -fold increase in Mmr1 levels in the absence of *dma1Δdma2Δ* (Figure S2).

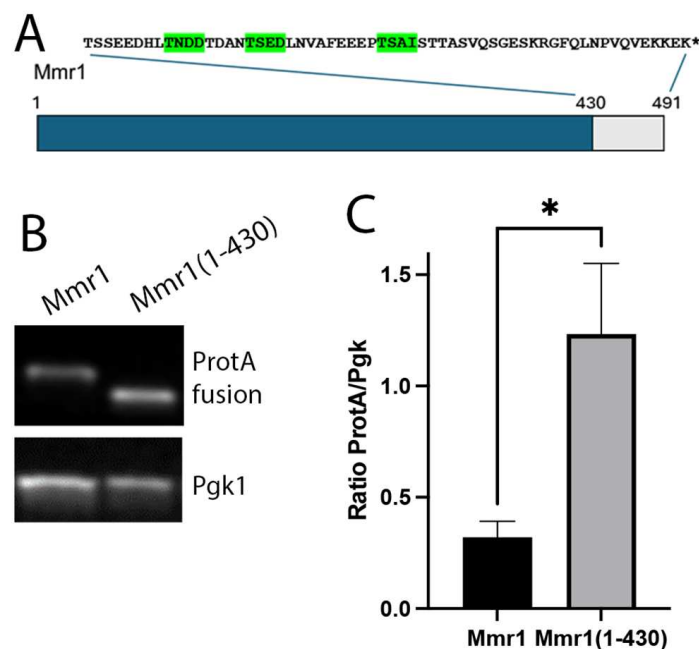


Figure 6. The role of the C-terminal region of Mmr1 in protein turnover. (A) A schematic diagram of Mmr1 showing the primary sequence of the C terminal 61 amino acids. Green highlights the putative Dma1/Dma2-interacting motifs. The predicted PEST region is 430–474. (B) Western blots of cell extracts over-expressing *DMA1* and Mmr1–Protein A or truncated Mmr1–Protein A were probed with antibodies to Protein A and PGK as a loading control. (C) The graph shows the relative levels of protein from three independent extract preps. Errors bars are SEM. Statistical test: unpaired *t*-test with Welch’s correction; * indicates *p* value of 0.0327.

3. Discussion

The genetic screen aimed to identify regulatory genes that when overexpressed affected mitochondrial organization and inheritance. While 90 of the initial 500 genes tested showed some changes in mitochondrial morphology, often these were also associated with dramatic changes in cell morphology or slow growth. Once these were discounted, 32 genes were re-examined for more detailed mitochondrial phenotypes with a focus on those that had reproducible inheritance phenotypes (examples in Figure 1). Importantly, and demonstrating the efficacy of the screen, a number of genes with previously identified links to the mitochondria were identified including *CLA4*, *DMA1*, *PCL7*, and *CQD1* [26,27,47]. There were also several known cell cycle genes such as *CDC26*, *SKP1/2*, and *CLB4*, which could indicate roles ensuring coupling between mitochondrial transport and the cell cycle [48]. Interestingly, blocking DNA replication does not prevent organelle inheritance, indicating that elements of regulation are maintained despite an S-phase cell cycle block [49].

Cla4 and *Dma1* have both previously been identified as having roles regulating organelle inheritance (reviewed in [3,5]). The current model proposes that early in the cell cycle, the myosin motor *Myo2* can bind to adaptors on the outer surface of organelles and, through movement on polarized actin filaments, deliver the organelles to the growing bud. Once in the bud, the adaptors are phosphorylated by *Cla4* kinase activity, and this leads to recognition by the ubiquitin ligases *Dma1* and *Dma2*. Following ubiquitination, the adaptors become substrates for the proteasomal degradation machinery.

Deletion of *CLA4* is known to lead to increased levels of adaptor proteins, including mitochondrial *Mmr1* [27], and overexpression of *CLA4* has been associated with premature *Vac17* degradation [50]; however, whether overexpression also impacts mitochondria has not been shown, and overexpression phenotypes are often more constrained by the availability of binding partners. Having generated an alternative overexpression construct to also demonstrate that the overexpression was *CLA4* specific, the effect on *Mmr1* levels was determined and, fitting with the model, resulted in a decrease in *Mmr1* levels. Unlike peroxisomes and vacuoles, mitochondrial inheritance is essential, and mitochondria cannot be synthesized de novo. Reflecting the essential requirement of inheritance, there appear to be partially redundant pathways to ensure mitochondrial inheritance. Not only is *Mmr1* a mitochondrial trafficking adaptor, but *Ypt11* and *Gem1* have also been ascribed a role in the transport. *Ypt11* is also an adaptor for the Golgi compartment inheritance and has been shown to bind to *Myo2* itself [31], while *Gem1* (a homologue of the mammalian *Miro*-GTPase) is an accessory factor for *ERMES* (ER Mitochondria Encounter Structures). *ERMES* are tethering sites that are involved in lipid fluxes between organelles [51,52]. There are also known to be other direct interactions of mitochondria, both with the ER via *Num1* and *MECA* (mitochondrial ER cortex anchor) complex [37,38] and with *Vps13* in contact sites at vacuoles [53]. Thus, one possibility is that mitochondria could be transported in an active, polarized manner to the bud through association with *Myo2* and *Mmr1* or *Ypt11* (Lewandowska et al., 2013). It is also possible that there is a low level of possibly passive movement of mitochondria into the bud mediated via interactions with various contact site complexes involved in lipid transport and quality control of mitochondria [34].

In order to disrupt the *Myo2* binding of *Mmr1*, an R409E mutation was generated based on the previous binding analysis of Tang and colleagues [28]. While the mutation did reduce binding as predicted, this was less dramatic in the context of the full-length protein compared to a fragment of the protein—amino acids 378–430 (Figure 3). Furthermore, the GFP-tagged *Mmr1*-R409E mutant was able to localize to the tip of the buds. This is in contrast to cells expressing a *myo2* I1308A mutant, which is impaired in *Mmr1* binding and does not support *Mmr1* nor mitochondrial transport to the bud [32]. In addition, to transport to the bud, *Mmr1*-R409E-GFP had a more intense signal, indicating increased protein levels. Additional experiments revealed that the *Mmr1* R409E mutant was more stable than its wild-type counterpart, even in the presence of elevated *Cla4* levels, indicating that the mutation rendered the protein resistant to *Cla4*-induced degradation. In silico modelling allows the charge distribution around the S414 phosphorylation site to be mapped. From

this, it is clear that the single R409E mutation has a profound impact on the surface that Cla4 would interface in order to gain access to the S414 site. It, therefore, suggests that, in vivo, the Mmr1 R409E mutation prevents phosphorylation by Cla4 and subsequent degradation of the protein. Further modelling also indicated that phosphorylation by Cla4 of Ser414 would be unlikely to lead directly to the disruption of the Mmr1-Myo2 complex, indicating the importance of other factors in this step of organelle transport termination.

The genetic screen also identified that overexpression of the ubiquitin ligase Dma1 could affect mitochondrial organization and inheritance. In this case, as predicted by the current working model, there were decreased levels of Mmr1 as judged by Mmr1-mNG signal intensities, and a delay in mitochondrial inheritance. However, levels of mitochondria, in fact, appeared to increase in large-budded cells (Figure S1). The reasons for this are not fully clear but one possibility is that the overexpression of *DMA1* leads to degradation of other factors involved in mitochondrial function, for example, in mitophagy. This would result in an accumulation of mitochondria overall as damaged organelles would not be removed and degraded. Future experiments could determine whether the accumulated and aggregated mitochondria maintained a membrane potential and functionality.

Dma1 and its paralogue Dma2 have been proposed to associate with adaptor proteins such as Mmr1 while in association with Myo2 in the mother cell, but only become active towards the adaptor following Cla4 phosphorylation [44]. Deletion of *DMA1* and *DMA2* is associated with increased levels of organelle adaptor proteins including Vac17 and Mmr1 [27,44,45]. We confirmed the effect of deleting the ubiquitin ligase genes on Mmr1 levels (Figure S3) and also showed that the Mmr1 most likely remains associated with Myo2 at the bud tip and then as it moves back towards the mother–bud neck region before cytokinesis [27]. To gain further insight into the region of Mmr1 important for Dma1 turnover, we deleted the C-terminal 61 amino acids of Mmr1, which contains both Dma1/2-binding and PEST motifs. The truncation did not, however, remove lysine K395, which has been identified as a ubiquitylated residue [54], allowing alternative binding ubiquitin ligases to potentially still function. The truncated Mmr1(1–430) was relatively stable, even to increased levels of Dma1 (Figure 6), indicating that the C-terminus of Mmr1 is the primary binding site for Dma1/2 ubiquitin ligase function.

Finally, an intriguing insight from the screen was the identification of both *PCL7* and *KIN4* as genes, which when overexpressed led to accumulations of Mmr1 at the bud tip region. Kin4 is a key protein in the spindle position checkpoint (SPoC) complex that determines when mitosis can be exited based on the appropriate position and inheritance of spindle pole bodies [55,56]. Kin4 has recently been proposed to function not only in SPB inheritance but more generally in other organelle inheritance patterns. One possibility is that Kin4 defines a spatial zone within the mother cell, which functions antagonistically to the role of Cla4 in the bud [45]. In terms of organelle adaptors, deletion of *KIN4* causes a decrease in adaptor protein levels, and kinase activity by Kin4 is proposed to serve a protective function while adaptors are in the mother cell. By extension, it might be predicted that overexpression of *KIN4* could lead to phosphorylation beyond its usual zone in the mother and could lead to protection of adaptors also in the bud. This could be one explanation of why there is an increase in Mmr1 at the bud tip observed in the screen. On the other hand, the Pcl7 cyclin functions in a complex with the Pho85 kinase [57,58]. Based on homology with other highly related kinases, it would be expected to phosphorylate serine residues in an -SP- motif and Mmr1 has four such motifs at Ser3, Ser16, Ser37, and Ser83. All of these serines have been identified in phospho-proteomic screens [54,59]. While the physiological relevance of *PCL7* overexpression on mitochondrial organization remains unclear, it is likely that high levels of *PCL7* could lead to phosphorylation at multiple sites in the N-terminal region of Mmr1. The Vac17 adaptor has been shown to be phosphorylated by another proline-directed serine kinase, Cdk1, and this is associated with Myo2 binding and subsequent transport to the bud [11]. By analogy, Mmr1 phosphorylation by Pcl7 could play a role in initiating Mmr1-Myo2 interaction and facilitating transport to the bud. In the

case of overexpression, continued high levels of Pcl7 could reduce the release of Mmr1 in the bud and so lead to the observed phenotypes.

The results show that a genetic overexpression screen was able to identify both known and novel genes that impact mitochondrial organization and inheritance. Further analysis of *CLA4* overexpression allowed us to identify two regions on Mmr1 important for the functional interaction with Cla4 and with Dma1. The identification of other kinases and phosphatases that impact mitochondrial inheritance could direct other studies that have shown the importance of Mmr1 but not Ypt11 in the selective inheritance of functional mitochondria [30], thus supporting the identification of regulators of the Mmr1-Myo2 interaction in mother cells.

4. Materials and Methods

4.1. Strains and Plasmids

S. cerevisiae strains used in this study are shown in Table S1. Yeast strains were derivatives of BY4741 (*MATA his3Δ1 leu2Δ0 met15Δ0 ura3Δ0*), which was obtained from the EUROSCARF consortium. BY4741 is referred to as wild-type (WT) cells and used as an isogenic control throughout the study.

Gene modifications or deletions were performed following the protocol described in [60]. The plasmids used in this study are shown in Table S2.

The mutagenesis method was as follows: After designing primers with the required nucleotide replacement, a linear fragment with the point mutation was generated using a proofreading DNA polymerase (Accuzyme™ polymerase; Bioline, Scientific Laboratory Supplies, Nottingham, UK). PCR products were co-transformed with a linearized plasmid for ligation in yeast using a high-efficiency transformation protocol. Individual colonies were grown in liquid cultures for genomic DNA isolation. Plasmid DNA was isolated via *E. coli* transformation followed by plasmid miniprep (Qiagen, Germantown, MD, USA). The constructed plasmid was sequenced to verify mutagenesis.

4.2. Yeast Growth Conditions

Cells were grown overnight and diluted to an OD₆₀₀ of 0.1 in the morning for all cell studies. Cells were then usually grown for a minimum of three hours before imaging. Yeast cells were grown at 30 °C in either of the following mediums: rich YPD medium (1% yeast extract, 2% peptone, and 2% glucose), minimal medium 2 (YM2) for the selection of the uracil prototrophic marker (2% glucose, 0.17% yeast nitrogen base without amino acids and ammonium sulphate, 0.5% ammonium sulphate, and 1% casamino acids), or minimal medium 1 (YM1) for the selection of all prototrophic markers (2% glucose, 0.17% yeast nitrogen base without amino acids and ammonium sulphate, and 0.5% ammonium sulphate). The appropriate amino acid stocks were added to the minimal medium as required.

4.3. Yeast Transformation

Yeast strains were grown overnight at 30 °C on a shaker at 200 rpm, in appropriate liquid media; YPD was used mostly. An amount of 200 μL from an overnight culture was centrifuged for 1 min at 12,000 rpm in an Eppendorf microfuge tube and the supernatant was discarded. Then, 1 μL of plasmid DNA (100–300 ng), 5 μL (50 μg) of single-stranded DNA (ssDNA), and 50 μL of one-step buffer (0.2 M Lithium Acetate pH 5.0, 40% (*w/v*) PEG (Polyethylene glycol) 3350, 0.1M DTT) were added to the pellet and mixed gently. Next, samples were incubated at room temperature for at least 3 hrs with regular mixing. Cells were then heat-shocked at 42 °C for 30 min and the cell suspension was plated on appropriate selective media. The plates were incubated at 30 °C for 2 days before colonies were selected.

4.4. Overexpression Screen

A library of gene overexpression strains was obtained from the Schuldiner lab (Weizmann Institute, Rehovot, Israel). The library was created using the SWAT method (SWAp-

Tag) [61] and consists of approximately 6000 strains in which the endogenous promoter was replaced by the strong TEF2 promoter and includes an N-terminal mCherry tag [43]. The Hettema lab created a sub-library containing 500 overexpressing strains. The selection of genes was based on those of other targeted screens and included kinases and phosphatases and their cofactors and phospho-binding proteins, ubiquitin ligases, ubiquitin ligase cofactors, and deubiquitylation factors. This sub-library was used and mated with strains that contain an ORF of interest tagged with the fluorescent protein mNeonGreen (mNG).

A schematic of the stages of the screen is shown in Figure S5. The library used for the mating was temporarily on the YPD–Clonat agar plate and plates were repinned on fresh YPD–Clonat agar plates and incubated for 2 days. Three 96-well (flat-bottom) plates were filled with 150 μ L of YPD using an 8-channel pipette. A 48-well pinner was used to transfer a small amount of the contents of the previously prepared fresh plates into the 96-well plates. The plates were incubated for 2 days at 30 °C. The strain carrying *MDH1-mNeonGreen* was grown overnight on medium lacking uracil. An amount of 70 mL of cell suspension was grown in YPD to $OD_{600} = 0.1$ and then transferred to a sterile Petri dish. An amount of 180 μ L of suspension was added to each well of 96-well (curved-bottom) plates. Finally, mating was performed using the library strains and the *MDH1-mNG* strain as follows: 20 μ L/well from the prepared library was added into each well of the plates prepared with the *MDH1-mNG* strain (curved-bottom plates). Plates were incubated for 2 days at 30 °C. Diploids were selected by pinning the cells on drop-out URA–Clonat agar plates. Then, plates were incubated at 30 °C for a further two days. Microscopic analysis of the mated library was as follows: the selected diploids were pinned into 96-well plates containing 150 μ L of selective medium and incubated overnight at 30 °C. The grown cells were diluted 1:20 in fresh medium in imaging plates and grown for 4 h. Imaging was performed using glass-bottom plates (ThermoFisher, Loughborough, UK).

4.5. Image Acquisition

Cells were analysed with a microscope (Axiovert 200M; Carl Zeiss, Oberkochen, Germany) equipped with an Exfo X-cite 120 excitation light source, bandpass filters (Carl Zeiss and Chroma Technology, Rockingham, VT, USA), an α Plan-Fluar 100 \times 1.45 NA and Plan-Apochromat 63 \times 1.4 NA objective lens (Carl Zeiss), and a digital camera (Orca ER; Hamamatsu Photonics, Hamamatsu City, Japan). Image acquisition was performed using Volocity software (version 6.1, PerkinElmer, Waltham, MA, USA). Fluorescence images were collected as 0.5 μ m z-stacks, merged into one plane using Openlab software (version 5.2.2, PerkinElmer), and processed further in Photoshop (Adobe, version 24.6). Bright-field images were collected in one plane. Each imaging experiment was performed at least three times, and representative images are shown. For quantitation, 2–3 experiments were used. Intensity and area measurements were carried out using Image J (version 1).

4.6. Yeast Two-Hybrid Analysis

S. cerevisiae strains PJ69-a and α [62] were transformed with GAL4 AD fusion constructs with a *LEU2* marker and with the indicated Gal4 BD fusion construct with a *TRP1* marker, respectively. Then, transformants were mated as follows: cells were grown on YPD agar overnight at 30 °C. Cells were scraped from agar plates and mixed with some Millipore sterile water. Then, each mating type was spotted on a fresh agar plate and incubated at 30 °C overnight. Next, the cells were harvested, resuspended in 40–50 μ L of selective liquid media, and spotted on selective solid media overnight at 30 °C. The mated strains were grown for 4–6 days at 30 °C on selective media -Leu-Irp. Beta-galactosidase assays were conducted as follows: An amount of 4–5 mL of cell culture was grown overnight. The next day, 1 ml from the overnight cell culture was spun at 2000 rpm for 2 min and the OD_{600} of the assayed culture was measured. The pellet was resuspended in 1 mL of Z buffer (solution of 200 mL consisting of 0.85% Na_2HPO_4 , 0.48% NaH_2PO_4 , 0.075% KCl, 0.0246% $MgSO_4 \cdot 7H_2O$, and 0.27% β -mercaptoethanol), which was pH adjusted to 7.0 before filter sterilizing. Approximately 3 drops of chloroform and 2 drops of 1% SDS were

added to the resuspended cells. The samples were vortexed at high speed for 1 min and then incubated at 28 °C for 5 min in the heating block before adding 0.2 mL of ONPG. The time was counted following ONPG addition and then the reaction was stopped when a pale-yellow colour was reached by adding 0.5 mL of Na₂CO₃. The samples were spun to obtain a clear supernatant to be measured for their OD₄₂₀. β-galactosidase activity was calculated using the following formula; the activity of β-galactosidase units was determined by measuring the O.D as the optical density of the reaction mix at 420 nm and at 600 nm for the original culture:

$$\text{OD}_{420\text{nm}}/\text{OD}_{600} \text{ of assayed culture} \times \text{volume assayed} \times \text{time (min)}$$

4.7. Protein Expression and Binding Analysis

For recombinant protein expression, 1 μL of plasmid was transformed into 30 μL of BL21 DE3 cells (ThermoFisher). Transformed cells were incubated overnight at 37 °C. An amount of 1 L of 2xTY culture with the selective antibiotic was grown using colonies scraped from the freshly transformed overnight plate. The culture was incubated at 37 °C until OD₆₀₀ = 0.8–0.9. An amount of 1 mM of the final concentration of IPTG was added to induce protein expression and the cells were incubated for another 3–4 h with shaking. Finally, the cells were harvested at 4 °C. The cell pellet was frozen and stored at –80 °C until protein purification.

The cell pellets were thawed on ice following resuspension in lysis buffer (1xPBS pH7.4, protease inhibitor without EDTA cocktail (Roche), 1 mM of DTT, and 15 μL of 50 mg/mL lysozyme). The cells were then broken by sonication using a 15 amplitude pulse 3 × 45 s on ice and 30 s off between each round. The cell lysate was cleared by centrifugation at 13,000 rpm for 40–45 min at 4 °C. To purify tagged proteins, the clear supernatant was transferred to Amylose (New England Biolabs, Hitchin, UK) or Glutathione Sepharose 4B (glutathione Sepharose 4B, Cytiva™, Merck, Gillingham, Dorset, UK). Beads were pre-equilibrated in wash buffer (1xPBS, 1% Tween, 300 mM NaCl) and added to the relevant fusion protein lysates. Lysates were incubated with the beads on a rotator at 4 °C for 30–60 min. After incubation, samples were spun at 3000 rpm in a benchtop clinical centrifuge for 3 min at 4 °C.

The in vitro binding assay was conducted as follows: MBP-Mmr1, Myo2 (cargo-binding domain)–GST protein fusions were expressed in *E. coli* BL21 DE3 and purified on Amylose or Glutathione Sepharose 4B beads prewashed in 1xPBS. After incubating the Myo2-GST or MBP-Mmr1 lysates with the relevant beads, samples were spun at 2000 g for 2 min, and the supernatant was collected in a new Eppendorf tube. The beads with the fusion proteins were washed 3–4 × with 10-bed volumes of wash buffer to remove non-specific binding material. The beads were spun between each wash at 3000 g for 3 min at 4 °C. The beads were washed 4 times with 1xPBS 300 mM NaCl. MBP-Mmr1 was eluted from amylose beads with maltose elution buffer (20 mM Tris-HCl pH 7.4, 200 mM NaCl, 1 mM EDTA, and 10 mM maltose). The *E. coli* lysates eluted were added to the GST-fusion bound beads. The samples were then incubated for 2 h at 4 °C with mixing. Next, the samples were spun at 2000 g for 2 min at 4 °C. The beads were washed 3–4 × with 10-bed volumes of 1xPBS + 300 mM NaCl. Then, an SDS-PAGE sample loading buffer was added and proteins were separated. Gels were stained using Coomassie staining or Western blotting.

4.8. Immunoblotting

For the preparation of extracts by alkaline lysis, cells were centrifuged, and pellets were resuspended in 0.2 M NaOH and 0.2% β-mercaptoethanol and left on ice for 10 min. The soluble protein was precipitated by the addition of 5% trichloroacetic acid and incubation on ice for 15 min. Following centrifugation (13,000 g, 5 min, 4 °C), the pellet was resuspended in 10 μL 1 M Tris-HCl (pH 9.4) and 90 μL 1 × SDS-PAGE sample loading buffer and boiled for 10 min at 95 °C. The samples (0.25–1OD₆₀₀ equivalent) were

resolved by SDS–PAGE followed by immunoblotting. Blots were blocked in 2% (*w/v*) fat-free dried milk in TBS containing Tween-20 [50 mM Tris-HCl pH 7.6, 150 mM NaCl, 0.1% (*v/v*) Tween-20]. GFP-tagged proteins were detected using a monoclonal anti-GFP antibody (mouse IgG monoclonal antibody clone 7.1 and 13.1; 1:3000; Roche (Basel, Switzerland), 11814460001). Mmr1–Protein A was detected by the peroxidase-anti peroxidase (PAP) antibody (rabbit; 1:4000; Sigma-Aldrich (Saint Louis, MO, USA), P1291). Pgk1 was detected by a monoclonal anti-Pgk1 antibody (mouse; 1:7000; Invitrogen (Carlsbad, CA, USA), 459250). Myo2-HA was detected by a monoclonal anti-HA antibody (mouse; 1:5000; Sigma-Aldrich, H9658). The secondary antibody was an HRP-linked anti-mouse polyclonal antibody (goat; 1:4000; Bio-Rad (Hercules, CA, USA), 1706516). Detection was achieved using enhanced chemiluminescence reagents (GE Healthcare, Waukesha, WI, USA) and chemiluminescence imaging.

4.9. Statistical Analysis

In the analysis of data, either a Student's *t*-test or ANOVA were used to assess significance. Tests used are indicated in figure legends and depend on the parameters of individual experiments. Data were plotted using GraphPad Prism 9.0.

4.10. In Silico Modelling

The basis for the structural modelling was the experimentally solved Myo2-Mmr1 crystal (structure identifier pdb 6IXP structure of the Myo2-cargo-binding domain (residues 1153–1574) in association with Mmr1 (residues 378–441)). Using Pymol 2.5.2, a mutation was introduced into the Mmr1 sequence R409E and the impact of that mutation on the electrostatic surface was modelled. Using the relevant post-translation modification plug-in on PyMol, a phosphate group was introduced to Ser37 in the Mmr1 peptide (corresponding to Ser414 in full-length Mmr1). The ePESTfind tool (<https://emboss.bioinformatics.nl/cgi-bin/emboss/pepfind>, accessed on 29 June 2023) was used to identify PEST sites.

Supplementary Materials: The following supporting information can be downloaded at: <https://www.mdpi.com/article/10.3390/kinasesphosphatases2020012/s1>. Table S1. Yeast strains used in this study. Table S2. Plasmids used in this study. Figure S1: Genes that affect mitochondrial morphology and inheritance when overexpressed. Figure S2. The localization of mitochondria in cells expressing Mmr1 R409E. Figure S3. The effect of *dma1* and *dma2* deletion on Mmr1. Figure S4. Identification of regions of Mmr1 important for degradation. Figure S5. Schematics explaining library construction and stages of genetic screening. Figure S6. Full blot images. References [32,61–63] are cited in the supplementary materials.

Author Contributions: Conceptualization, E.H.H.; Formal analysis, N.N. and K.R.A.; Investigation, N.N.; Methodology, N.N., L.E., E.H.H. and K.R.A.; Resources, L.E., N.N. and E.H.H.; Supervision, E.H.H. and K.R.A.; Validation, N.N., K.R.A. and E.H.H.; Writing—original draft, K.R.A.; Writing—review and editing, N.N., L.E., E.H.H. and K.R.A.; Funding acquisition, N.N. and L.E. All authors have read and agreed to the published version of the manuscript.

Funding: This research was funded by the Civil Service Commission of Kuwait to N.N and the Vice Chancellor's Indian Scholarship awarded to L.E. by The University of Sheffield, UK.

Institutional Review Board Statement: Not applicable.

Informed Consent Statement: Not applicable.

Data Availability Statement: All data are contained in the manuscript and Supplementary Materials.

Acknowledgments: We would like to thank Maya Schuldiner (Weizmann Institute) for providing the overexpression library.

Conflicts of Interest: The authors declare no conflicts of interest.

References

1. Knoblach, B.; Rachubinski, R.A. Sharing the cell's bounty-organelle inheritance in yeast. *J. Cell Sci.* **2015**, *128*, 621–630. [[CrossRef](#)]

2. Ménasché, G.; Pastural, E.; Feldmann, J.; Certain, S.; Ersoy, F.; Dupuis, S.; Wulffraat, N.; Bianchi, D.; Fischer, A.; Le Deist, F.; et al. Mutations in RAB27A cause Griscelli syndrome associated with haemophagocytic syndrome. *Nat. Genet.* **2000**, *25*, 173–176. [[CrossRef](#)]
3. Obara, K.; Nishimura, K.; Kamura, T. E3 Ligases Regulate Organelle Inheritance in Yeast. *Cells* **2024**, *13*, 292. [[CrossRef](#)]
4. Warren, G.; Wickner, W. Organelle inheritance. *Cell* **1996**, *84*, 395–400. [[CrossRef](#)]
5. Wong, S.; Weisman, L.S. Let it go: Mechanisms that detach myosin V from the yeast vacuole. *Curr. Genet.* **2021**, *67*, 865–869. [[CrossRef](#)]
6. Motley, A.M.; Hettema, E.H. Yeast peroxisomes multiply by growth and division. *J. Cell Biol.* **2007**, *178*, 399–410. [[CrossRef](#)]
7. Jin, Y.; Weisman, L.S. The vacuole/lysosome is required for cell-cycle progression. *Elife* **2015**, *4*, e08160. [[CrossRef](#)]
8. McConnell, S.J.; Stewart, L.C.; Talin, A.; Yaffe, M.P. Temperature-sensitive yeast mutants defective in mitochondrial inheritance. *J. Cell Biol.* **1990**, *111*, 967–976. [[CrossRef](#)]
9. Klecker, T.; Westermann, B. Asymmetric inheritance of mitochondria in yeast. *Biol. Chem.* **2020**, *401*, 779–791. [[CrossRef](#)] [[PubMed](#)]
10. Nunnari, J.; Walter, P. Regulation of organelle biogenesis. *Cell* **1996**, *84*, 389–394. [[CrossRef](#)] [[PubMed](#)]
11. Peng, Y.; Weisman, L.S. The cyclin-dependent kinase Cdk1 directly regulates vacuole inheritance. *Dev. Cell* **2008**, *15*, 478–485. [[CrossRef](#)] [[PubMed](#)]
12. Fagarasanu, A.; Mast, F.D.; Knoblach, B.; Jin, Y.; Brunner, M.J.; Logan, M.R.; Glover, J.N.; Eitzen, G.A.; Aitchison, J.D.; Weisman, L.S.; et al. Myosin-driven peroxisome partitioning in *S. cerevisiae*. *J. Cell Biol.* **2009**, *186*, 541–554. [[CrossRef](#)] [[PubMed](#)]
13. Pruyne, D.; Legesse-Miller, A.; Gao, L.; Dong, Y.; Bretscher, A. Mechanisms of polarized growth and organelle segregation in yeast. *Annu. Rev. Cell Dev. Biol.* **2004**, *20*, 559–591. [[CrossRef](#)] [[PubMed](#)]
14. Estrada, P.; Kim, J.; Coleman, J.; Walker, L.; Dunn, B.; Takizawa, P.; Novick, P.; Ferro-Novick, S. Myo4p and She3p are required for cortical ER inheritance in *Saccharomyces cerevisiae*. *J. Cell Biol.* **2003**, *163*, 1255–1266. [[CrossRef](#)]
15. Shepard, K.A.; Gerber, A.P.; Jambhekar, A.; Takizawa, P.A.; Brown, P.O.; Herschlag, D.; DeRisi, J.L.; Vale, R.D. Widespread cytoplasmic mRNA transport in yeast: Identification of 22 bud-localized transcripts using DNA microarray analysis. *Proc. Natl. Acad. Sci. USA* **2003**, *100*, 11429–11434. [[CrossRef](#)] [[PubMed](#)]
16. Govindan, B.; Bowser, R.; Novick, P. The Role of Myo2, a Yeast Class V Myosin, in Vesicular Transport. *J. Cell Biol.* **1995**, *128*, 1055–1068. [[CrossRef](#)] [[PubMed](#)]
17. Schott, D.; Ho, J.; Pruyne, D.; Bretscher, A. The COOH-terminal domain of Myo2p, a yeast myosin V, has a direct role in secretory vesicle targeting. *J. Cell Biol.* **1999**, *147*, 791–808. [[CrossRef](#)] [[PubMed](#)]
18. Catlett, N.L.; Duex, J.E.; Tang, F.; Weisman, L.S. Two distinct regions in a yeast myosin-V tail domain are required for the movement of different cargoes. *J. Cell Biol.* **2000**, *150*, 513–526. [[CrossRef](#)] [[PubMed](#)]
19. Catlett, N.L.; Weisman, L.S. The terminal tail region of a yeast myosin-V mediates its attachment to vacuole membranes and sites of polarized growth. *Proc. Natl. Acad. Sci. USA* **1998**, *95*, 14799–14804. [[CrossRef](#)]
20. Hill, K.L.; Catlett, N.L.; Weisman, L.S. Actin and myosin function in directed vacuole movement during cell division in *Saccharomyces cerevisiae*. *J. Cell Biol.* **1996**, *135*, 1535–1549. [[CrossRef](#)]
21. Rossanese, O.W.; Reinke, C.A.; Bevis, B.J.; Hammond, A.T.; Sears, I.B.; O'Connor, J.; Glick, B.S. A role for actin, Cdc1p, and Myo2p in the inheritance of late Golgi elements in *Saccharomyces cerevisiae*. *J. Cell Biol.* **2001**, *153*, 47–62. [[CrossRef](#)] [[PubMed](#)]
22. Simon, V.R.; Pon, L.A. Actin-based organelle movement. *Experientia* **1996**, *52*, 1117–1122. [[CrossRef](#)] [[PubMed](#)]
23. Hoepfner, D.; van den Berg, M.; Philippsen, P.; Tabak, H.F.; Hettema, E.H. A role for Vps1p, actin, and the Myo2p motor in peroxisome abundance and inheritance in *Saccharomyces cerevisiae*. *J. Cell Biol.* **2001**, *155*, 979–990. [[CrossRef](#)] [[PubMed](#)]
24. Tang, F.; Kauffman, E.J.; Novak, J.L.; Nau, J.J.; Catlett, N.L.; Weisman, L.S. Regulated degradation of a class V myosin receptor directs movement of the yeast vacuole. *Nature* **2003**, *422*, 87–92. [[CrossRef](#)] [[PubMed](#)]
25. Weisman, L.S. Organelles on the move: Insights from yeast vacuole inheritance. *Nat. Rev. Mol. Cell. Biol.* **2006**, *7*, 243–252. [[CrossRef](#)] [[PubMed](#)]
26. Yau, R.G.; Wong, S.; Weisman, L.S. Spatial regulation of organelle release from myosin V transport by p21-activated kinases. *J. Cell Biol.* **2017**, *216*, 1557–1566. [[CrossRef](#)] [[PubMed](#)]
27. Obara, K.; Yoshikawa, T.; Yamaguchi, R.; Kuwata, K.; Nakatsukasa, K.; Nishimura, K.; Kamura, T. Proteolysis of adaptor protein Mmr1 during budding is necessary for mitochondrial homeostasis in *Saccharomyces cerevisiae*. *Nat. Commun.* **2022**, *13*, 2005. [[CrossRef](#)]
28. Tang, K.; Li, Y.; Yu, C.; Wei, Z. Structural mechanism for versatile cargo recognition by the yeast class V myosin Myo2. *J. Biol. Chem.* **2019**, *294*, 5896–5906. [[CrossRef](#)] [[PubMed](#)]
29. Pernice, W.M.; Vevea, J.D.; Pon, L.A. A role for Mfb1p in region-specific anchorage of high-functioning mitochondria and lifespan in *Saccharomyces cerevisiae*. *Nat. Commun.* **2016**, *7*, 10595. [[CrossRef](#)]
30. Chelius, X.; Bartosch, V.; Rausch, N.; Haubner, M.; Schramm, J.; Braun, R.; Klecker, T.; Westermann, B. Selective retention of dysfunctional mitochondria during asymmetric cell division. *PLoS Biol.* **2023**, *21*, e3002310. [[CrossRef](#)]
31. Chernyakov, I.; Santiago-Tirado, F.; Bretscher, A. Active segregation of yeast mitochondria by Myo2 is essential and mediated by Mmr1 and Ypt11. *Curr. Biol.* **2013**, *23*, 1818–1824. [[CrossRef](#)]
32. Eves, P.T.; Jin, Y.; Brunner, M.; Weisman, L.S. Overlap of cargo binding sites on myosin V coordinates the inheritance of diverse cargoes. *J. Cell Biol.* **2012**, *198*, 69–85. [[CrossRef](#)]

33. Förtsch, J.; Hummel, E.; Krist, M.; Westermann, B. The myosin-related motor protein Myo2 is an essential mediator of bud-directed mitochondrial movement in yeast. *J. Cell Biol.* **2011**, *194*, 473–488. [[CrossRef](#)]
34. Buvelot Frei, S.; Rahl, P.B.; Nussbaum, M.; Briggs, B.J.; Calero, M.; Janeczko, S.; Regan, A.D.; Chen, C.Z.; Barral, Y.; Whittaker, G.R.; et al. Bioinformatic and comparative localization of Rab proteins reveals functional insights into the uncharacterized GTPases Ypt10p and Ypt11p. *Mol. Cell. Biol.* **2006**, *26*, 7299–7317. [[CrossRef](#)]
35. Frederick, R.L.; Okamoto, K.; Shaw, J.M. Multiple pathways influence mitochondrial inheritance in budding yeast. *Genetics* **2008**, *178*, 825–837. [[CrossRef](#)]
36. Lewandowska, A.; Macfarlane, J.; Shaw, J.M. Mitochondrial association, protein phosphorylation, and degradation regulate the availability of the active Rab GTPase Ypt11 for mitochondrial inheritance. *Mol. Biol. Cell* **2013**, *24*, 1185–1195. [[CrossRef](#)]
37. Pernice, W.M.; Swayne, T.C.; Boldogh, I.R.; Pon, L.A. Mitochondrial Tethers and Their Impact on Lifespan in Budding Yeast. *Front. Cell Dev. Biol.* **2017**, *5*, 120. [[CrossRef](#)]
38. Westermann, B. Mitochondrial inheritance in yeast. *Biochim. Biophys. Acta* **2014**, *1837*, 1039–1046. [[CrossRef](#)]
39. Kruppa, A.J.; Buss, F. Motor proteins at the mitochondria-cytoskeleton interface. *J. Cell Sci.* **2021**, *134*, jcs226084. [[CrossRef](#)]
40. Mehta, A.D.; Rock, R.S.; Rief, M.; Spudich, J.A.; Mooseker, M.S.; Cheney, R.E. Myosin-V is a processive actin-based motor. *Nature* **1999**, *400*, 590–593. [[CrossRef](#)]
41. Sato, O.; Sakai, T.; Choo, Y.Y.; Ikebe, R.; Watanabe, T.M.; Ikebe, M. Mitochondria-associated myosin 19 processively transports mitochondria on actin tracks in living cells. *J. Biol. Chem.* **2022**, *298*, 101883. [[CrossRef](#)] [[PubMed](#)]
42. Kruppa, A.J.; Kishi-Itakura, C.; Masters, T.A.; Rorbach, J.E.; Grice, G.L.; Kendrick-Jones, J.; Nathan, J.A.; Minczuk, M.; Buss, F. Myosin VI-Dependent Actin Cages Encapsulate Parkin-Positive Damaged Mitochondria. *Dev. Cell* **2018**, *44*, 484–499. [[CrossRef](#)]
43. Weill, U.; Yofe, I.; Sass, E.; Stynen, B.; Davidi, D.; Natarajan, J.; Ben-Menachem, R.; Avihou, Z.; Goldman, O.; Harpaz, N.; et al. Genome-wide SWAp-Tag yeast libraries for proteome exploration. *Nat. Methods* **2018**, *15*, 617–622. [[CrossRef](#)]
44. Yau, R.G.; Peng, Y.; Valiathan, R.R.; Birkeland, S.R.; Wilson, T.E.; Weisman, L.S. Release from myosin V via regulated recruitment of an E3 ubiquitin ligase controls organelle localization. *Dev. Cell* **2014**, *28*, 520–533. [[CrossRef](#)]
45. Ekal, L.; Alqahtani, A.M.S.; Schuldiner, M.; Zalckvar, E.; Hettema, E.H.; Ayscough, K.R. Spindle Position Checkpoint Kinase Kin4 Regulates Organelle Transport in *Saccharomyces cerevisiae*. *Biomolecules* **2023**, *13*, 1098. [[CrossRef](#)]
46. Itoh, T.; Toh, E.A.; Matsui, Y. Mmr1p is a mitochondrial factor for Myo2p-dependent inheritance of mitochondria in the budding yeast. *EMBO J.* **2004**, *23*, 2520–2530. [[CrossRef](#)]
47. Khosravi, S.; Chelius, X.; Unger, A.K.; Rieger, D.; Frickel, J.; Sachsenheimer, T.; Lüchtenborg, C.; Schieweck, R.; Brügger, B.; Westermann, B.; et al. The UbiB family member Cqd1 forms a novel membrane contact site in mitochondria. *J. Cell Sci.* **2023**, *136*, jcs260578. [[CrossRef](#)]
48. Leite, A.C.; Costa, V.; Pereira, C. Mitochondria and the cell cycle in budding yeast. *Int. J. Biochem. Cell Biol.* **2023**, *161*, 106444. [[CrossRef](#)]
49. Li, K.W.; Lu, M.S.; Iwamoto, Y.; Drubin, D.G.; Pedersen, R.T.A. A preferred sequence for organelle inheritance during polarized cell growth. *J. Cell Sci.* **2021**, *134*, jcs258856. [[CrossRef](#)]
50. Bartholomew, C.R.; Hardy, C.F. p21-activated kinases Cla4 and Ste20 regulate vacuole inheritance in *Saccharomyces cerevisiae*. *Eukaryot. Cell* **2009**, *8*, 560–572. [[CrossRef](#)] [[PubMed](#)]
51. Guillén-Samander, A.; Leonzino, M.; Hanna, M.G.; Tang, N.; Shen, H.; De Camilli, P. VPS13D bridges the ER to mitochondria and peroxisomes via Miro. *J. Cell Biol.* **2021**, *220*, e202010004. [[CrossRef](#)] [[PubMed](#)]
52. Wozny, M.R.; Di Luca, A.; Morado, D.R.; Picco, A.; Khaddaj, R.; Campomanes, P.; Ivanović, L.; Hoffmann, P.C.; Miller, E.A.; Vanni, S.; et al. In situ architecture of the ER-mitochondria encounter structure. *Nature* **2023**, *618*, 188–192. [[CrossRef](#)] [[PubMed](#)]
53. Bean, B.D.M.; Dziurdzik, S.K.; Kolehmainen, K.L.; Fowler, C.M.S.; Kwong, W.K.; Grad, L.I.; Davey, M.; Schluter, C.; Conibear, E. Competitive organelle-specific adaptors recruit Vps13 to membrane contact sites. *J. Cell Biol.* **2018**, *217*, 3593–3607. [[CrossRef](#)] [[PubMed](#)]
54. Swaney, D.L.; Beltrao, P.; Starita, L.; Guo, A.; Rush, J.; Fields, S.; Krogan, N.J.; Villén, J. Global analysis of phosphorylation and ubiquitylation cross-talk in protein degradation. *Nat. Methods* **2013**, *10*, 676–682. [[CrossRef](#)] [[PubMed](#)]
55. D’Aquino, K.E.; Monje-Casas, F.; Paulson, J.; Reiser, V.; Charles, G.M.; Lai, L.; Shokat, K.M.; Amon, A. The protein kinase Kin4 inhibits exit from mitosis in response to spindle position defects. *Mol. Cell* **2005**, *19*, 223–234. [[CrossRef](#)] [[PubMed](#)]
56. Pereira, G.; Schiebel, E. Kin4 kinase delays mitotic exit in response to spindle alignment defects. *Mol. Cell* **2005**, *19*, 209–221. [[CrossRef](#)] [[PubMed](#)]
57. Lee, M.; O’Regan, S.; Moreau, J.L.; Johnson, A.L.; Johnston, L.H.; Goding, C.R. Regulation of the Pcl7-Pho85 cyclin-cdk complex by Pho81. *Mol. Microbiol.* **2000**, *38*, 411–422. [[CrossRef](#)] [[PubMed](#)]
58. Measday, V.; Moore, L.; Retnakaran, R.; Lee, J.; Donoviel, M.; Neiman, A.M.; Andrews, B. A family of cyclin-like proteins that interact with the Pho85 cyclin-dependent kinase. *Mol. Cell. Biol.* **1997**, *17*, 1212–1223. [[CrossRef](#)] [[PubMed](#)]
59. Lanz, M.C.; Yugandhar, K.; Gupta, S.; Sanford, E.J.; Faça, V.M.; Vega, S.; Joiner, A.M.N.; Fromme, J.C.; Yu, H.; Smolka, M.B. In-depth and 3-dimensional exploration of the budding yeast phosphoproteome. *EMBO Rep.* **2021**, *22*, e51121. [[CrossRef](#)]
60. Longtine, M.S.; McKenzie, A.; Demarini, D.J.; Shah, N.G.; Wach, A.; Brachat, A.; Philippsen, P.; Pringle, J.R. Additional modules for versatile and economical PCR-based gene deletion and modification in *Saccharomyces cerevisiae*. *Yeast* **1998**, *14*, 953–961. [[CrossRef](#)]

61. Yofe, I.; Weill, U.; Meurer, M.; Chuartzman, S.; Zalckvar, E.; Goldman, O.; Ben-Dor, S.; Schütze, C.; Wiedemann, N.; Knop, M.; et al. One library to make them all: Streamlining the creation of yeast libraries via a SWAp-Tag strategy. *Nat. Methods* **2016**, *13*, 371–378. [[CrossRef](#)] [[PubMed](#)]
62. James, P.; Halladay, J.; Craig, E.A. Genomic libraries and a host strain designed for highly efficient two-hybrid selection in yeast. *Genetics* **1996**, *144*, 1425–1436. [[CrossRef](#)] [[PubMed](#)]
63. Pashkova, N.; Jin, Y.; Ramaswamy, S.; Weisman, L.S. Structural basis for myosin V discrimination between distinct cargoes. *EMBO J.* **2006**, *25*, 693–700. [[CrossRef](#)] [[PubMed](#)]

Disclaimer/Publisher’s Note: The statements, opinions and data contained in all publications are solely those of the individual author(s) and contributor(s) and not of MDPI and/or the editor(s). MDPI and/or the editor(s) disclaim responsibility for any injury to people or property resulting from any ideas, methods, instructions or products referred to in the content.